



# When can the local advection–dispersion equation simulate non-Fickian transport through rough fractures?

Lizhi Zheng<sup>1</sup> · Lichun Wang<sup>2</sup> · Scott C. James<sup>3</sup>

Published online: 4 March 2019

© Springer-Verlag GmbH Germany, part of Springer Nature 2019

## Abstract

Non-Fickian solute transport is observed across many scales, which has motivated development of numerous non-Fickian-based models. Assuming that local fluid flow was estimable from the Modified Local Cubic Law, this study determined whether the local ADE better simulated non-Fickian transport through rough (3-D) fractures when local dispersion was described using either the Taylor dispersion coefficient ( $D_{\text{Taylor}}$ ) or the molecular diffusion coefficient ( $D_m$ ). The assessment was based on how well the local ADE compared to particle-tracking solutions for solute transport across a range of Péclet numbers ( $Pe$ ) through two simulated fractures. Even though the local ADE is based on local Fickian transport processes, it was able to reproduce non-Fickian transport characteristics through these heterogeneous fractures. When supplying  $D_{\text{Taylor}}$  to the local ADE, it extended the applicability of the local ADE to a threshold of  $Pe < 450$ ; using  $D_m$ , the local ADE was only accurate when  $Pe < 70$ . No differences were observed for small  $Pe$ . Therefore, our recommendation is to always use  $D_{\text{Taylor}}$  in the local ADE to capture non-Fickian transport so long as the  $Pe$  threshold is not exceeded.

**Keywords** Non-Fickian transport · Local advection–dispersion equation · Fracture flow · Particle tracking · Taylor dispersion

## 1 Introduction

Non-Fickian transport has been observed in porous and fractured media from the pore scale to the kilometer scale (Berkowitz et al. 2006; Dentz et al. 2011; Maxwell et al. 2016). Although many experiments, numerical simulations, and theoretical analysis have been designed to interrogate non-Fickian transport, accurate prediction of non-Fickian transport in heterogeneous geological media remains challenging (Neuman and Tartakovsky 2009; Cadini et al. 2013; Shih 2004).

Broadly speaking, two approaches have been used to quantify non-Fickian transport (Dogan et al. 2014).

- (1) The family of non-Fickian transport theories including: the multi-rate mass transfer model (Haggerty and Gorelick 1995), the mobile-immobile model (Gao et al. 2010; Zhang et al. 2014), continuous-time random-walk models (Berkowitz et al. 2006), and time fractional-derivative models (Garrard et al. 2017). Unlike the classical advection–dispersion equation (ADE), these non-Fickian theories have parameters that lack solid physical bases. This has motivated efforts to establish connections between these parameters and measurable physical properties (Wang and Cardenas 2014).
- (2) The local ADE. The macroscopic ADE fails to simulate non-Fickian transport because it lacks the necessary physics to represent the true heterogeneity of the system (Berkowitz et al. 2006; Wang and Cardenas 2014). To overcome this deficiency, researchers proposed the local ADE method (Fiori et al. 2013; Hanna and Rajaram 1998) where the ADE is applied with each model cell individually parameterized according to its local flow and dispersion. The local ADE method has successfully reproduced non-

✉ Lichun Wang  
wanglichun@tju.edu.cn

<sup>1</sup> Department of Geological Sciences, University of Texas at Austin, Austin, TX 78712, USA

<sup>2</sup> Institute of Surface-Earth System Science, Tianjin University, Tianjin 300072, China

<sup>3</sup> Department of Geoscience and Mechanical Engineering, Baylor University, Waco, TX 76798, USA

Fickian transport observed at the Macrodispersion Experiment site in Columbus (Mississippi, USA) (Dogan et al. 2014). Also, simulations using the local ADE are appealing because they are computationally efficient (Dogan et al. 2014; Fiori et al. 2013).

Although the local ADE is a viable model for simulating non-Fickian transport in heterogeneous porous media (Dogan et al. 2014), it has yet to be fully demonstrated for transport through rough-walled (3-D) fractures (Deng et al. 2015; Detwiler and Rajaram 2007; Elkhoury et al. 2013; Hanna and Rajaram 1998). To close this knowledge gap, this study established the conditions (defined by the Péclet number) under which the local ADE can accurately simulate transport processes within heterogeneous fractures when non-Fickian transport behavior is prominent.

## 2 Methodology

To assess the applicability of the local ADE for simulating transport through heterogeneous fractures, it was compared to the demonstrably accurate random-walk particle-tracking (RWPT) model (Wang and Cardenas 2015). Two natural heterogeneous fractures were scanned and used to build demonstration models. By gradually increasing the pressure gradient, the applicability of the local ADE was assessed with increasing Péclet number:

$$Pe = \frac{u\langle b \rangle}{D_m} \quad (1)$$

where  $u$  (m/s) is mean fluid velocity,  $\langle b \rangle$  (m) is the arithmetic mean of the aperture field, and  $D_m = 2.03 \times 10^{-9}$  m<sup>2</sup>/s is the molecular diffusion coefficient.

### 2.1 Fracture descriptions

Flow and transport models were built for two rough fractures described previously (Wang et al. 2015). These two fractured Santana tuff samples were scanned at the X-ray computed tomography (HRXCT) facility at the University of Texas at Austin (Ketcham et al. 2010; Slottke 2010). Fracture A (Fig. 1a) had horizontal and vertical resolutions of 0.26 and 0.25 mm, respectively. Fracture B (Fig. 1b) had horizontal and vertical resolutions of 0.28 and 0.25 mm, respectively. Table 1 provides the fracture physical characteristics.

Both aperture fields approximate a lognormal distribution with  $\langle b \rangle$  equal to 3.35 and 1.50 mm for Fractures A and B, respectively. Aperture correlation lengths,  $\lambda_b$  (m), were calculated using the geostatistical simulator SGeMS

(Remy et al. 2009) by fitting an exponential model to the experimental semivariograms of  $b$  with a nugget effect.

### 2.2 The local ADE model

Flow and transport processes through 3-D fractures are described by the Navier–Stokes equations (NSE) and the advection–diffusion equation, respectively (Wang and Cardenas 2015). However, directly resolving solute transport in a fracture is computationally costly, especially for high Reynolds number ( $Re$ ) that requires a fine mesh size (Wang and Cardenas 2015; Zimmerman et al. 2004). For computational expediency, flow and transport processes are often estimated using efficient depth-averaged models (Nicholl et al. 1999), i.e., a quasi-3D approach.

#### 2.2.1 The steady-state depth-averaged flow model

Fluid flow through fractures depends on fracture heterogeneity (i.e., fracture roughness and tortuosity) and flow regimes (Brush and Thomson 2003; Zimmerman et al. 2004). Flow through parallel plates is described by the Cubic Law (Witherspoon et al. 1980); it was extended to fractures with moderate roughness as the Local Cubic Law (Nicholl et al. 1999; Wang et al. 2015). Here, an updated version called the Modified Local Cubic Law (MLCL) (Wang et al. 2015) was used to resolve steady flows through the fractures. The MLCL, which can improve the numerical solution for steady flow by simultaneously incorporating fracture roughness, tortuosity, and weak inertial forces, is:

$$\nabla \cdot \left[ \frac{T_x}{M} \frac{\partial p}{\partial x} \cos(\phi_x) \vec{i} + \frac{T_y}{M} \frac{\partial p}{\partial y} \cos(\phi_y) \vec{j} \right] = 0 \quad (2)$$

where  $T_x$  and  $T_y$  are transmissivities based on local aperture field in the  $x$  and  $y$  directions,  $p$  is pressure,  $\phi_x$  and  $\phi_y$  are the local flow orientation angles based on the knowledge of local tortuosity in the  $x$  and  $y$  directions, and  $M$  is a correction coefficient that accounts for the effects of local fracture roughness and weak inertial forces (Wang et al. 2015). The MLCL is demonstrably robust at the local scale because the MLCL: (1) reproduces total discharge calculated from the NSE and (2) preserves local flux calculated by vertically integrating the velocity field from the NSE (Wang et al. 2015).

Constant pressures were specified at the inlet (left) and outlet (right) as shown in Fig. 2, driving longitudinal ( $x$ -direction) flow; top and bottom boundaries were assigned zero flux. Pressure gradients were increased yielding  $Re$  ranging from 0.003 to 0.94 for Fracture A and 0.002 to 0.90 for Fracture B:

**Fig. 1** Aperture fields for Fractures **(a)** A and **(b)** B. Probability density distributions (PDDs) of log-apertures for Fractures **(c)** A and **(d)** B

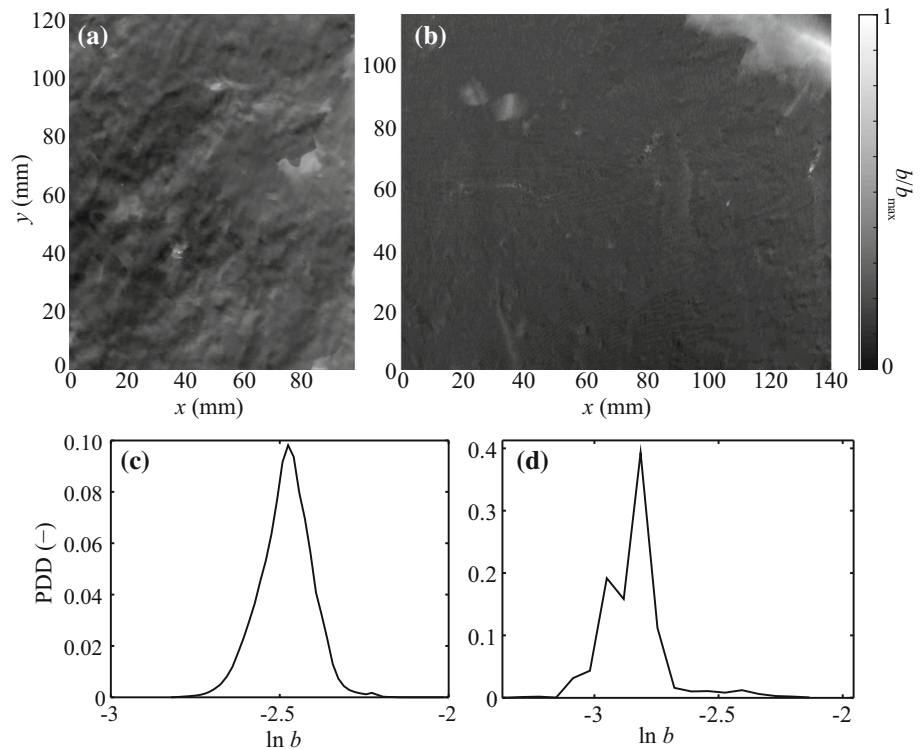


**Table 1** Aperture-field characteristics for Fractures A and B with flow and transport regimes described by  $Re$  and  $Pe$

Fracture	$\langle b \rangle$ (mm)	$\sigma_b$ (mm)	$\lambda_b$ (mm)	$\nabla P$ (Pa/m)	$Re$ (-)	$Pe$ (-)
Fracture A	3.35	0.60	60	0.001–0.36	0.003–0.94	1.32–461.26
Fracture B	1.50	0.59	30	0.001–4.29	0.002–0.90	0.74–445.56

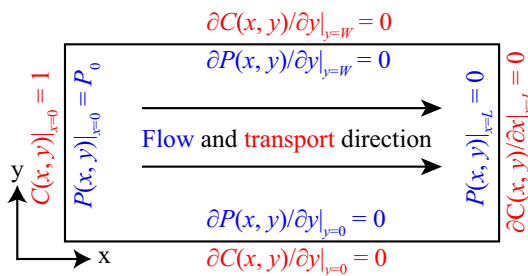


**Fig. 2** Schematic of the flow (blue) and transport (red) models

$$Re = \frac{\rho Q}{W\mu} \tag{3}$$

where  $\rho$  (1000 kg/m<sup>3</sup>) is fluid density,  $Q$  (m<sup>3</sup>) is discharge from the MLCL, and  $W$  (m) is fracture width, and  $\mu$  (10<sup>-3</sup> Pa-s) is fluid dynamic viscosity. All simulations were within the Darcy flow regime, because flow transition generally occurs where  $Re > 1$  and this is when inertial effects are non-negligible.

Flow fields were simulated with a MatLab finite-difference routine by solving pressure and fluid-flux fields using the MLCL (James et al. 2018), upon which transport

processes were estimated through solution of the local ADE and by the RWPT model.

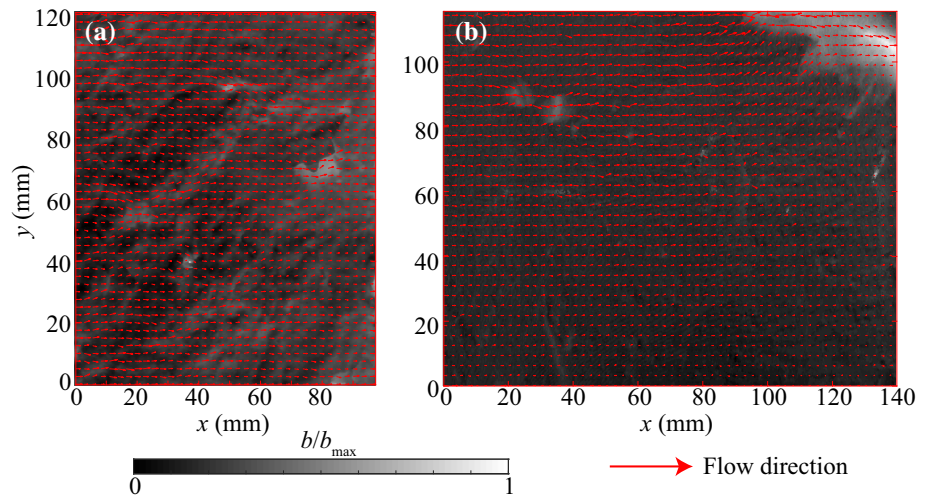
### 2.2.2 The depth-averaged transport (local ADE) model

The flow field governs solute advection and dispersion (Fischer et al. 1979). In addition to depth-averaged flux fields ( $\mathbf{q} = [q_x, q_y]$ , where  $q_x$  and  $q_y$  fluxes in the  $x$  and  $y$  directions, respectively) from the MLCL, spatially variable dispersion coefficients are required by the local ADE:

$$\frac{\partial(bC)}{\partial t} + \nabla \cdot (\mathbf{q}C) = \nabla \cdot (b\mathbf{D}\nabla C) \tag{4}$$

where  $C$  (-) is depth-averaged normalized concentration,  $t$  (s) is time, and  $\mathbf{D}$  (m/s<sup>2</sup>) is the 2-D, spatially varying dispersion coefficient. Initial concentrations were zero. Along the inlet boundary,  $C = 1$ , while the outlet was assigned an open boundary condition with zero diffusive/dispersive flux such that solutes exited only by advective flux (Fig. 2). The top and bottom boundaries were no-flux. The local ADE was solved with a Matlab finite-difference model. Numerical instabilities were minimized with a first-order upwind scheme for the advection term and a second-

**Fig. 3** Flow fields for fractures (a) A and (b) B. The gray scale indicates  $b$  with maximum aperture,  $b_{max}$ , and red arrows indicate local flow directions



order central difference approximation for the dispersion term (Slingerland and Kump 2011).

Because the velocity field was assumed accurate (Wang et al. 2015), the validity of the local ADE solution was assessed using two different methods to specify  $\mathbf{D}$  in Eq. (4) using either  $D_m$  or  $D_{Taylor}$ , which combines molecular diffusion with the effects of velocity gradients on solute spreading (Detwiler and Rajaram 2007; James and Chrysikopoulos 1999, 2000):

$$D_{Taylor} = \begin{bmatrix} D_m + \frac{q_x^2}{210D_m} & 0 \\ 0 & D_m + \frac{q_y^2}{210D_m} \end{bmatrix} \quad (5)$$

Note that Taylor dispersion theory is only valid upon exceeding specific length or time thresholds (Fischer et al. 1979; Wang et al. 2012). Prior to such thresholds, pre-asymptotic dispersion is observed (Bolster et al. 2014; Meng and Yang 2016; Wang et al. 2012), but not considered here. Because length/time thresholds grow with increasing  $Pe$ , and the fracture length was fixed, increasing  $Pe$  could lead to violation of the assumptions in Taylor dispersion theory. This work identified under what  $Pe$  regimes  $D_m$  or  $D_{Taylor}$  can be successfully used in the local ADE to capture non-Fickian transport in rough fractures.

### 2.3 The RWPT model

The quasi-3D RWPT model simulates transport through heterogeneous fractures (James et al. 2005; James and Chrysikopoulos 2001) by updating particle locations  $[x, y, z]$  each time step:

$$\begin{aligned} x^{n+1} &= x^n + u\Delta t + N(0, 1)\sqrt{2D_m\Delta t} \\ y^{n+1} &= y^n + v\Delta t + N(0, 1)\sqrt{2D_m\Delta t} \\ z^{n+1} &= z^n + w\Delta t + N(0, 1)\sqrt{2D_m\Delta t} \end{aligned} \quad (6)$$

where  $n$  and  $n + 1$  represent present and future time steps,  $\Delta t$  is an adaptive time interval that balances computational efficiency and solution accuracy (Wang and Cardenas 2015),  $[u, v, w]$  are velocities in the  $[x, y, z]$  directions,

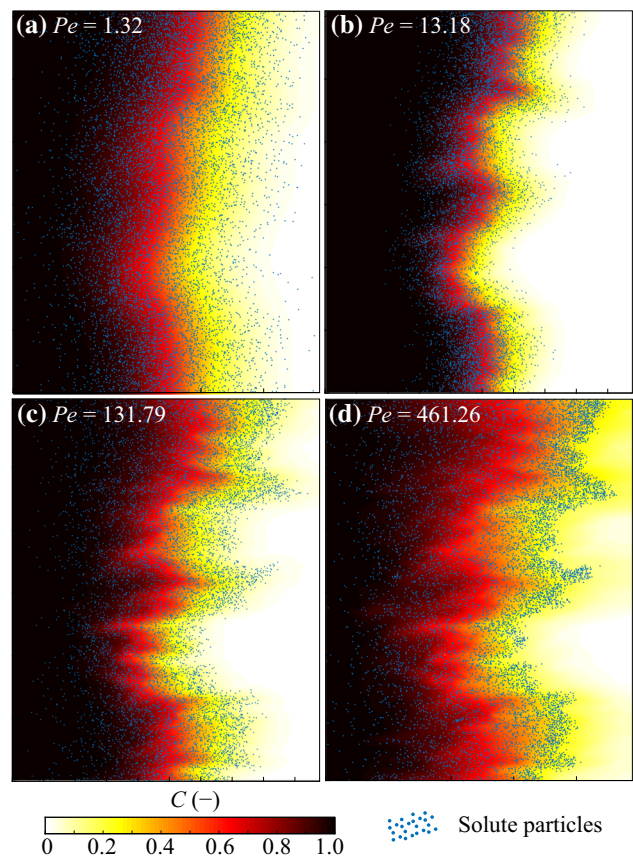


**Fig. 4** Transport snapshots for Fracture A at pore volume (PV, defined as time  $\times$  discharge/fracture volume) = 0.5 with increasing  $Pe$  from (a)–(d). The colored field is the solution to the local ADE using  $D_{Taylor}$  while dots are the solution from the RWPT model

respectively, and  $N(0, 1)$  is an independent selection from the standard normal distribution.

Note that  $u$  and  $v$  were calculated as a function of  $z$  according to the parabolic velocity profile (James et al. 2005). Mass was conserved by specifying  $[q_x, q_y]$  during vertical integrations of  $u$  and  $v$ , respectively, which resulted in  $w = 0$  everywhere. The absence of advection in the  $z$  direction was compensated for by adjusting particle's  $z$  location when it flowed across adjacent cells according to mid-surface plane variations; which mimicked the fracture-normal flow component (i.e., mid-surface plane tortuosity). Like direct NSE solutions in 3D fractures, RWPT solutions were assumed appropriate for assessing the applicability of the local ADE.

Effluent solute concentrations from the RWPT model were calculated as:

$$C_{RWPT} = \frac{n(t)}{N} \tag{7}$$

where  $n(t)$  (–) is the cumulative number of particles exiting fracture over time and  $N = 10^4$  is the total number of particles injected into the fractures and apportioned according to the local flux. The RWPT model was solved with a parallelized MatLab routine; solutions were insensitive to any further increase in  $N$  (not shown).

### 3 Results and discussion

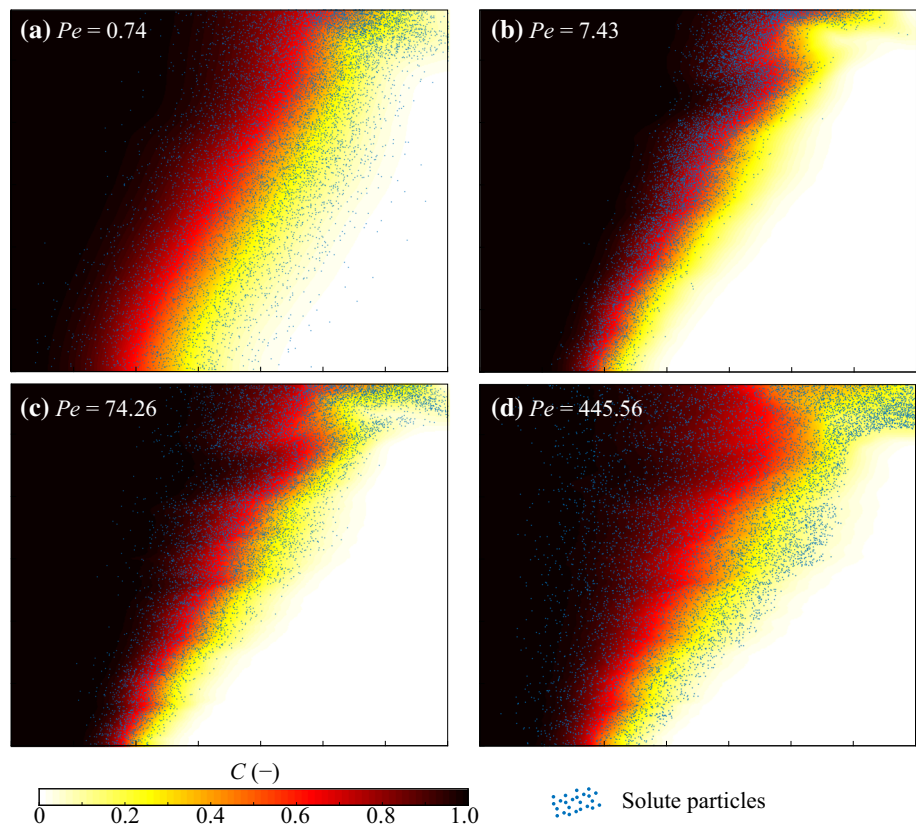
#### 3.1 Flow fields

Figure 3 shows the resulting flow field; neither aperture field was sufficiently variable (rough) to yield preferential flow paths because apparent roughness,  $\sigma_b/\langle b \rangle < 0.4$  where  $\sigma_b$  is the standard deviation of  $b$ . Gradual trends in the aperture fields directed regional flow toward larger aperture zones (more conductive areas) as evident, for example, in the flow toward the upper corner of Fracture B in Fig. 3. This trend in the velocity field notably affected overall transport process leading to non-Fickian transport.

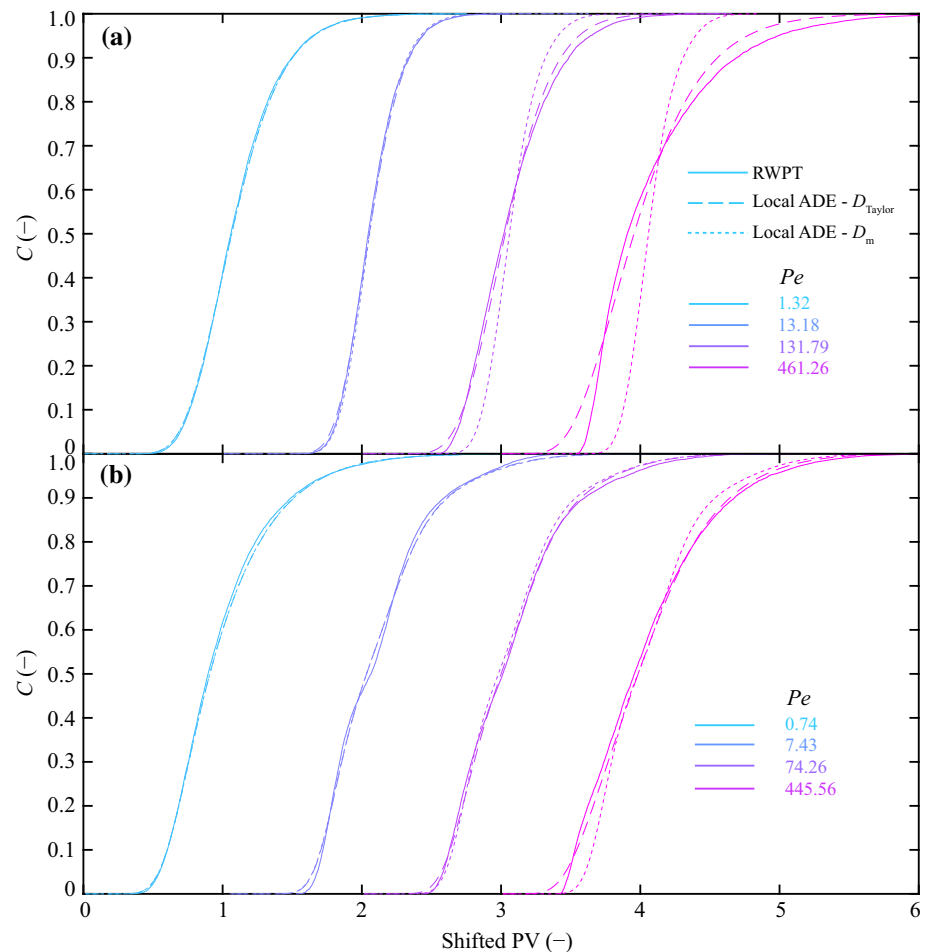
#### 3.2 Non-Fickian transport

Non-Fickian transport process must be present when breakthrough curves (BTCs) cannot be replicated with the Fickian-based macroscopic ADE (Berkowitz et al. 2006). For spatially correlated, heterogeneous fractures, non-Fickian transport is expected when fracture length,  $L$ , is less than  $20\lambda_b$  to  $25\lambda_b$  (Detwiler et al. 2002; Wang and Cardenas 2017), which holds true for the fractures considered here (Table 1). Moreover, aperture trends led to the uneven plume fronts evident in Figs. 4 and 5 for all  $Re$  and  $Pe$  regimes. Uneven plume evolution resulted in non-Fickian

**Fig. 5** Transport snapshots through Fracture B at  $PV = 0.5$  with increasing  $Pe$  from (a)–(d). The colored field is the solution to the local ADE using  $D_{Taylor}$  while dots are the solution from the RWPT model



**Fig. 6** BTCs with increasing  $Pe$  for Fractures (a) A and (b) B from the RWPT model (solid curves), the local ADE using  $D_{Taylor}$  (long-dashed curves), and the local ADE using  $D_m$  (short-dashed curves). Note that each curve with a given  $Pe$  is shifted by one PV



transport typified by the early arrival and heavy tailing in the BTCs evident in the solid curves in Fig. 6. The degree of non-Fickian transport increased with  $Pe$  as demonstrated by increased heavy tailing (solid curves in Fig. 6).

### 3.3 Assessment of the local ADE in capturing non-Fickian transport

Applicability of the local ADE was assessed with increasing  $Pe$ . Indeed, the effects of  $Pe$  on the validity of the local ADE were considered here because of an analogous macrodispersion study (Detwiler et al. 2000), which suggested that the dispersion regimes transition from molecular diffusion to Taylor dispersion with increasing  $Pe$ .

Figure 6 compares RWPT BTCs to solutions from the local ADE when either  $D_m$  or  $D_{Taylor}$  was supplied for  $\mathbf{D}$ . Both solutions degraded with increasing  $Pe$ . Specifically, when  $Pe < 70$ , the local ADE using  $D_{Taylor}$  and  $D_m$  both could faithfully reproduce RWPT plume characteristics (Figs. 4, 5) and BTCs (Fig. 6). This was expected, because  $D_{Taylor}$  approaches  $D_m$  as  $Pe$  decreases (Detwiler

et al. 2000; Wang et al. 2012). Upon increasing  $Pe > 70$ , the local ADE with  $D_m$  was not able to satisfactorily capture non-Fickian transport.

To extend the applicability of the local ADE to higher  $Pe$ ,  $D_{Taylor}$  calculated using the local aperture of the model cell was used for  $\mathbf{D}$  to consider mechanical dispersion. It is not intuitive that this should work because as  $Pe$  increases, so do both  $D_{Taylor}$  and the length threshold for it to be applicable (but this cannot change for a fixed model cell size) (Wang et al. 2012). Interestingly, when using  $D_{Taylor}$ , the local ADE was accurate for  $Pe < 450$  (Fig. 6). This implies that  $D_{Taylor}$  should always be used in the local ADE because it extends the range of applicability to higher  $Pe$  regimes ( $Pe < 450$ ).

## 4 Implications

Accurately simulating non-Fickian transport in hydrology remains challenging due to strong heterogeneities (Neuman and Tartakovsky 2009). While many non-Fickian-based models have been proposed to simulate non-Fickian

transport, the physical meanings of related parameters remain elusive (Berkowitz et al. 2006). The validity of the process-based local ADE has not been thoroughly interrogated for fractured media exhibiting non-Fickian transport, although it has been validated for porous media (Dogan et al. 2014; Fiori et al. 2013). This study recommends use of model-cell-based  $D_{\text{Taylor}}$  for the spatially variable dispersion coefficient in the local ADE for transport regimes with  $Pe < 450$ .

## 5 Conclusions

Although the computationally efficient local ADE can capture non-Fickian transport in porous media, its applicability to transport through rough fractures has been under-explored. Here, the range of applicability of the local ADE was extended by using the local Taylor dispersion coefficient rather than the molecular diffusion coefficient. The range of applicability of the local ADE was extended from  $Pe < 70$  when using  $D_m$  to  $Pe < 450$  when using  $D_{\text{Taylor}}$ , suggesting that  $D_{\text{Taylor}}$  should always be used in the local ADE. The local ADE with  $D_{\text{Taylor}}$  under appropriate  $Pe$  regimes is able to capture and predict non-Fickian transport in fractured media.

**Acknowledgements** This work is financially supported by National Key R&D Program of China (Grant No. 2016YFA0601002). Additional financial support is provided by the Geology Foundation of the University of Texas and by Tianjin University.

## References

- Berkowitz B et al (2006) Modeling non-Fickian transport in geological formations as a continuous time random walk. *Rev Geophys* 44:RG2003
- Bolster D et al (2014) Modeling preasymptotic transport in flows with significant inertial and trapping effects—the importance of velocity correlations and a spatial Markov model. *Adv Water Resour* 70:89–103
- Brush DJ, Thomson NR (2003) Fluid flow in synthetic rough-walled fractures: Navier–Stokes, Stokes, and local cubic law simulations. *Water Resour Res* 39:1085
- Cadini F, De Sanctis J, Bertoli I, Zio E (2013) Upscaling of a dual-permeability Monte Carlo simulation model for contaminant transport in fractured networks by genetic algorithm parameter identification. *Stoch Environ Res Risk Assess* 27:505–516
- Deng H et al (2015) Alterations of fractures in carbonate rocks by CO<sub>2</sub>-acidified brines. *Environ Sci Technol* 49:10226–10234
- Dentz M et al (2011) Mixing, spreading and reaction in heterogeneous media: a brief review. *J Contam Hydrol* 120–121:1–17
- Detwiler RL, Rajaram H (2007) Predicting dissolution patterns in variable aperture fractures: evaluation of an enhanced depth-averaged computational model. *Water Resour Res* 43:W04403
- Detwiler RL et al (2000) Solute transport in variable-aperture fractures: an investigation of the relative importance of Taylor dispersion and macrodispersion. *Water Resour Res* 36:1611–1625
- Detwiler RL et al (2002) Experimental and simulated solute transport in a partially-saturated, variable-aperture fracture. *Geophys Res Lett* 29:113-1–113-4
- Dogan M et al (2014) Predicting flow and transport in highly heterogeneous alluvial aquifers. *Geophys Res Lett* 41:7560–7565
- Elkhoury JE et al (2013) Dissolution and deformation in fractured carbonates caused by flow of CO<sub>2</sub>-rich brine under reservoir conditions. *Int J Greenh Gas Control* 16:S203–S215
- Fiori A et al (2013) The plume spreading in the MADE transport experiment: could it be predicted by stochastic models? *Water Resour Res* 49:2497–2507
- Fischer HB et al (1979) Mixing in inland and coastal waters. Academic, San Diego
- Gao G et al (2010) A new mobile-immobile model for reactive solute transport with scale-dependent dispersion. *Water Resour Res* 46
- Garrard RM et al (2017) Can a time fractional-derivative model capture scale-dependent dispersion in saturated soils? *Groundwater* 55:857–870
- Haggerty R, Gorelick SM (1995) Multiple-rate mass transfer for modeling diffusion and surface reactions in media with pore-scale heterogeneity. *Water Resour Res* 31:2383–2400
- Hanna RB, Rajaram H (1998) Influence of aperture variability on dissolutional growth of fissures in Karst Formations. *Water Resour Res* 34:2843–2853
- James SC, Chrysikopoulos CV (1999) Transport of polydisperse colloid suspensions in a single fracture. *Water Resour Res* 35:707–718
- James SC, Chrysikopoulos CV (2000) Transport of polydisperse colloids in a saturated fracture with spatially variable aperture. *Water Resour Res* 36:1457–1465
- James SC, Chrysikopoulos CV (2001) An efficient particle tracking equation with specified spatial step for the solution of the diffusion equation. *Chem Eng Sci* 56:6535–6543
- James SC et al (2005) Contaminant transport in a fracture with spatially variable aperture in the presence of monodisperse and polydisperse colloids. *Stoch Environ Res Risk Assess* 19:266–279
- James SC et al (2018) Modeling colloid transport in fractures with spatially variable aperture and surface attachment. *J Hydrol* 566:735–742
- Ketcham RA et al (2010) Three-dimensional measurement of fractures in heterogeneous materials using high-resolution X-ray computed tomography. *Geosphere* 6:499–514
- Maxwell RM et al (2016) The imprint of climate and geology on the residence times of groundwater. *Geophys Res Lett* 43:701–708
- Meng X, Yang D (2016) Determination of dynamic dispersion coefficient for particles flowing in a parallel-plate fracture. *Colloid Surf A* 509:259–278
- Neuman SP, Tartakovsky DM (2009) Perspective on theories of non-Fickian transport in heterogeneous media. *Adv Water Resour* 32:670–680
- Nicholl MJ et al (1999) Saturated flow in a single fracture: evaluation of the Reynolds equation in measured aperture fields. *Water Resour Res* 35:3361–3373
- Remy N et al (2009) Applied geostatistics with SGeMS: a user's guide. Cambridge University Press, Cambridge
- Shih D-F (2004) Uncertainty analysis: one-dimensional radioactive nuclide transport in a single fractured media. *Stoch Environ Res Risk Assess* 18:198–204
- Slingerland R, Kump L (2011) Mathematical modeling of earth's dynamical systems: a primer. Princeton University Press, Princeton
- Slotke DT (2010) Surface roughness of natural rock fractures: implications for prediction of fluid flow. Geological sciences, Vol. Ph.D. The University of Texas at Austin, Texas, Austin

- Wang L, Cardenas MB (2017) Transition from non-Fickian to Fickian longitudinal transport through 3-D rough fractures: scale-(in)sensitivity and roughness dependence. *J Contam Hydrol* 198:1–10
- Wang L, Cardenas MB (2014) Non-Fickian transport through two-dimensional rough fractures: assessment and prediction. *Water Resour Res* 50:871–884
- Wang L, Cardenas MB (2015) An efficient quasi-3D particle tracking-based approach for transport through fractures with application to dynamic dispersion calculation. *J Contam Hydrol* 179:47–54
- Wang L et al (2012) Theory for dynamic longitudinal dispersion in fractures and rivers with Poiseuille flow. *Geophys Res Lett* 39:L05401
- Wang L et al (2015) Modification of the local cubic law of fracture flow for weak inertia, tortuosity, and roughness. *Water Resour Res* 51:2064–2080
- Witherspoon PA et al (1980) Validity of cubic law for fluid flow in a deformable rock fracture. *Water Resour Res* 16:1016–1024
- Zhang Y et al (2014) Linking aquifer spatial properties and non-Fickian transport in mobile-immobile like alluvial settings. *J Hydrol* 512:315–331
- Zimmerman RW et al (2004) Non-linear regimes of fluid flow in rock fractures. *Int J Rock Mech Min Sci* 41(Supplement 1):163–169

**Publisher's Note** Springer Nature remains neutral with regard to jurisdictional claims in published maps and institutional affiliations.